Eur. Phys. J. D **27**, 43–53 (2003)
DOI: 10.1140/epjd/e2003-00234-2

THE EUROPEAN PHYSICAL JOURNAL D

Orbital magnetism in axially deformed sodium clusters

From scissors mode to dia-para magnetic anisotropy

V.O. Nesterenko[1,a], W. Kleinig[1,2], P.-G. Reinhard[3], N. Lo Iudice[4], F.F. de Souza Cruz[5], and J.R. Marinelli[5]

[1] Bogoliubov Laboratory of Theoretical Physics, Joint Institute for Nuclear Research, Dubna, Moscow region 141980, Russia
[2] Technische Universität Dresden, Institut für Analysis, 01062 Dresden, Germany
[3] Institut für Theoretische Physik, Universität Erlangen, 91058 Erlangen, Germany
[4] Dipartimento di Scienze Fisiche, Università di Napoli "Federico II" and Istituto Nazionale di Fisica Nucleare, Dipartamento di Scienze Fisiche, Monte S. Angelo, Via Cinthia, 80126 Napoli, Italy
[5] Departamento de Fisica, Universidade Federal de Santa Catarina, Florianópolis, SC 88040-900, Brazil

Received 20 December 2002
Published online 29 July 2003 –

Abstract. Low-energy orbital magnetic dipole excitations, known as the scissors mode (SM), are studied in alkali metal clusters. Subsequent dynamic and static effects are explored. The treatment is based on a self-consistent microscopic approach using the jellium approximation for the ionic background and the Kohn-Sham mean field for the electrons. The microscopic origin of SM and its main features (structure of the mode in light and medium clusters, separation into low- and high-energy plasmons, coupling high-energy M1 scissors and E2 quadrupole plasmons, contributions of shape isomers, etc.) are discussed. It is shown that the scissors M1 strength acquires large values with increasing cluster size. The mode is responsible for the van Vleck paramagnetism of spin-saturated clusters. Quantum shell effects induce a fragile interplay between Langevin diamagnetism and van Vleck paramagnetism and lead to a remarkable dia-para anisotropy in magnetic susceptibility of particular light clusters. Finally, several routes for observing the SM experimentally are discussed.

PACS. 36.40.-c Atomic and molecular clusters – 36.40.Cg Electronic and magnetic properties of clusters – 36.40.Gk Plasma and collective effects in clusters – 36.40.Vz Optical properties of clusters

1 Introduction

Investigation of orbital magnetism in atomic clusters (see, *e.g.*, [1–6]) has been of considerable interest in recent years. Because of a possibly large number of atoms in a cluster, the valence electrons can accede single-particle orbitals with very high angular momenta. The occupation of these orbitals has strong impact on cluster static magnetism (see, *e.g.* [1–3] and references therein) and collective magnetic modes of orbital nature [1,4–6]. Two remarkable examples are the scissors [1,4,5] and twist [6] modes. The scissors mode (SM) is strictly correlated with cluster deformation. It can be viewed as a small-amplitude rotational oscillation of a spheroid of valence electrons against a spheroid of the ionic background (hence the name SM).

The SM is a general dynamic phenomenon already found or predicted in different finite quantum systems. It was first proposed [7] and observed [8] in atomic nuclei where it still remains a hot topic for both experimental and theoretical studies (for a review see [9]). It was later predicted in a variety of different systems, like metal clusters [1,4], quantum dots [10] and ultra-cold superfluid gas of fermionic atoms [11]. More remarkably, it was predicted [12] and observed [13] in a Bose-Einstein condensate. All these different systems have two features in common: broken spherical symmetry and a two-component nature (neutrons and protons in nuclei, valence electrons and ions in atomic clusters, electrons and surrounding media in quantum dots, atoms and the trap in dilute Fermi gas and Bose condensate).

The orbital magnetism in alkali metal clusters is described in terms of Langevin diamagnetism and van Vleck paramagnetism [1,2]. They are both weak and, therefore, need to be studied in systems where strong forms of magnetism, like ferromagnetism, are absent. Alkali metal clusters provide here a good testing ground. The SM strongly affects the orbital magnetism. Being a low-energy mode, the SM determines the van Vleck paramagnetism and causes a strong anisotropy in the magnetic susceptibility [1,14]. Moreover, particular light clusters can exhibit dia-para anisotropy, being diamagnetic along z-symmetry axis and paramagnetic in x-, y-directions [14].

The SM has already been studied with schematic [1] and microscopic [4,14,15] approaches. The microscopic

[a] e-mail: nester@thsun1.jinr.ru

calculations, though accounting for quantum shells effects, were not fully self-consistent. A deformed Woods-Saxon [16], rather than a self-consistent Kohn-Sham, one-body potential was adopted. The quadrupole deformation was deduced from other models or experimental estimates. Certainly, we need to perform fully self-consistent calculations based on the density-functional theory in order to settle the subtle issues, like the fragile dia-para anisotropy, the role of the ionic structure, triaxiality, shape isomers, etc.

In this connection, we present a thorough study of different SM issues, based on the LDA Kohn-Sham functional. This study not only checks out and refines the previously obtained results (which as such is important because of the subtle character of some effects) but also leads to new ones. For example, investigation of the role of shape isomers demonstrates that the SM in clusters with $N > 50$ is in fact a statistical mix of contributions from different cluster shapes. This conclusion is important for the analysis of possible ways for the experimental observation of the SM. The thorough discussion of experimental perspectives is a further essential and new point of the paper.

Self-consistent calculations accounting for the ionic structure were performed for spin-saturated ground and spin-polarized isomeric states of light sodium clusters Na_{12} and Na_{16} [5]. It was found that the scissors response remains determined basically by the global deformation, in spite of the fact that triaxiality and ionic structure induce a strong fragmentation in the strength. It was also shown that the detailed ionic structure destroys locally spherical symmetry thereby causing a finite, though very weak, M1 response (transverse optical mode) even in clusters with zero global deformation.

Calculations of the same level of completeness become prohibitive as one moves to heavier clusters. For this reason, we are forced to use in the present paper the Kohn-Sham approach with a soft jellium model for the ionic background [17]. This simplifies greatly the calculations and allows one to proceed to heavier clusters. At the same time, the jellium approach is accurate enough for the principal problems considered here. The treatment of the electrons is fully self-consistent. We adopt a deformed Kohn-Sham mean field using the energy functional with the Gunnarsson-Lundqvist exchange-correlation term [18]. The cluster shape (in terms of axial quadrupole and hexadecapole deformations) is determined by varying the jellium deformation and minimizing the total energy of the system. The optical response in the linear regime is calculated within the separable random-phase-approximation (SRPA) method [19,20] self-consistently derived from the Kohn-Sham functional. The method has been already successfully employed for the description of the dipole plasmon in spherical [21] and deformed [20,22] alkali metal clusters.

In the present paper, we will consider both the optical M1 response and static magnetic orbital effects. In Section 2, macroscopic and microscopic treatments of the SM are briefly outlined. In Section 3, the calculation scheme is presented. The optical response is discussed in Sections 4 and 5. It will be shown that, in analogy with the electric dipole plasmon in deformed clusters [20,22], the M1 response in light clusters has a distinctive profile determined by the deformation. Instead, due to a strong Landau damping and contributions of shape isomers, the response in medium clusters becomes vague and the SM can be viewed as a statistical mix of contributions from different cluster shapes. Besides, we discuss structure of the residual interaction and explain a small collective shift in SM excitations. The coupling between the high-energy SM branch and the electric quadrupole plasmon is demonstrated. In Section 6, the dia-para anisotropy is discussed. In Section 7, we estimate perspectives to observe the SM in photo-absorption, Raman scattering and inelastic electron scattering. The conclusions are given in Section 8.

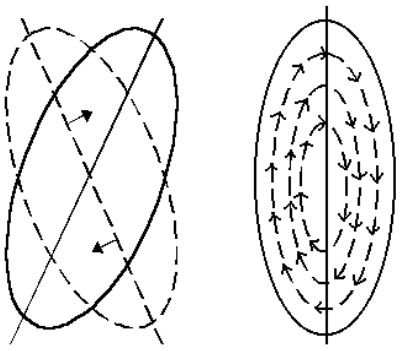

Fig. 1. Macroscopic view of scissors mode: rigid rotation [7] (left), and rotation within a rigid surface [1] (right).

2 The scissors mode: brief outline

The macroscopic and microscopic treatments of the SM in clusters are discussed in detail in references [1,4,5]. Thus, we give here only a brief outline for a better understanding of the results presented in the next sections.

In the geometrical model of [7], the SM arises from rotational oscillations of valence electrons *versus* the ions, both assumed to form distinct spheroids (see left part of Fig. 1). Following the alternative view of [1] (right part of Fig. 1), the displacement field of the mode is a sum of the rigid rotation and the quadrupole term (the latter provides vanishing velocity of electrons at the surface):

$$\mathbf{u}(\mathbf{r}) = \boldsymbol{\Omega} \times \mathbf{r} + \delta_2(1 + \delta_2/3)^{-1}\nabla(yz) \qquad (1)$$

where δ_2 is the quadrupole deformation parameter (to be defined in the next section). Both macroscopic treatments, [1,7], include the rigid rotation of valence electrons *versus* the ions with the restoring force originating from the Coulomb interaction between the electrons and ions. The treatment [1] has the additional quadrupole term which changes the character of the restoring force. It originates there not from the Coulomb interaction but from distortions of the Fermi sphere in the momentum space thus manifesting the elastic behavior of the system (see [1] for the detailed discussion). As was shown

in [4], the microscopic calculations give the SM energy and strength very close to the macroscopic estimates [1], see equations (2, 3) below.

In axially symmetric systems, the SM is generated by the orbital momentum fields, L_x and L_y, perpendicular to the symmetry axis z and is characterized by the quantum numbers $|\Lambda^\pi = 1^+\rangle$ where Λ is the eigenvalue of L_z and π is the space parity. Energy and magnetic strength of the mode can be estimated macroscopically [1,4]:

$$\omega = \frac{20.7}{r_s^2} N_e^{-1/3} \delta_2 \text{ eV}, \tag{2}$$

$$\begin{aligned} B(M1) &= 4\langle 1^+ \mid \hat{L}_x \mid 0\rangle^2 \mu_b^2 \\ &= \frac{2}{3} N_e \overline{r^2} \omega \mu_b^2 \\ &\simeq N_e^{4/3} \delta_2 \ \mu_b^2 \end{aligned} \tag{3}$$

where N_e is the number of valence electrons in the cluster, r_s is the Wigner-Seitz radius (in Å), and μ_b is the Bohr magneton. We use here natural units $m_e = \hbar = c = 1$. The value $B(M1)$ stands for the summed strength of the degenerated x- and y-branches. The z-branch vanishes for symmetry reasons. It is worth noting that $B(M1)$ does not depend on r_s and so is the same for different metals.

The microscopic treatment of the SM takes into account the shell structure of the axially deformed mean field. One can characterize the emerging single electron states in terms of the quantum numbers of the axially deformed harmonic oscillator (Clemenger-Nilsson basis). These are the triplets $\nu = [\mathcal{N} n_z \Lambda]$ where n_z labels the number of nodes in z-direction (= symmetry axis), and $\mathcal{N}$ is the principle shell number $\mathcal{N} = n_z + 2n_r + \Lambda$ (from which one can derive the number n_r of radial nodes). The angular momenta orthogonal to the symmetry axis, $\hat{L}_x$ and $\hat{L}_y$, promote low-energy $\Delta\mathcal{N} = 0$ transitions inside the valence shell and high-energy $\Delta\mathcal{N} = 2$ transitions across two shells. One may expand the single-electron wave functions in the spherical basis $(nL\Lambda)$

$$\Psi_{\nu=[\mathcal{N} n_z \Lambda]} = \sum_{nL} a_{nL}^{\nu} R_{nL}(r) Y_{L\Lambda}(\Omega) \tag{4}$$

and then to evaluate the orbital M1 transition amplitude between hole ($\nu = h$) and particle ($\nu = p$) states as

$$\begin{aligned} \langle \Psi_p | \hat{L}_x | \Psi_h \rangle \propto \delta_{\pi_p,\pi_h} \delta_{\Lambda_p,\Lambda_h \pm 1} \\ \times \sum_{nL} a_{nL}^p a_{nL}^h \sqrt{L(L+1) - \Lambda_h(\Lambda_h \pm 1)}. \end{aligned} \tag{5}$$

Equation (5) shows that the scissors mode is generated by $\Lambda_p = \Lambda_h \pm 1$ transitions between the components of one and the same spherical (nL)-level. In spherical systems, $(nL\Lambda)$-states of the level (nL) are degenerate by Λ while in deformed systems they exhibit the deformation splitting and so may be connected by M1 transitions with non-zero excitation energies. This is the origin of the scissors mode. The energy scale of the scissors mode is determined by the deformation energy splitting and so is rather small. This explains the predominantly low-energy ($\Delta\mathcal{N} = 0$) character of the scissors mode. Just the low-energy branch carries most of the scissors $B(M1)$ strength (see also discussion in Sect. 4). The high-energy ($\Delta\mathcal{N} = 2$) branch of the mode is much weaker since the particle states involved into ($\Delta\mathcal{N} = 2$) transitions include only small (nL)-components from the valence shell.

Table 1. Ground state deformation parameters δ_2 and δ_4 and moments β_2 and β_4. For Na_{55}^+ and Na_{119}^+ the deformation parameters for the isomeric states together with their energy deficits ΔE are also given.

Cluster	δ_2	δ_4	β_2	β_4	ΔE, eV
Na_{11}^+	0.355	0.25	0.44	0.41	-
Na_{15}^+	0.59	–0.19	0.47	–0.02	-
Na_{19}^+	–0.285	–0.09	–0.21	–0.02	-
Na_{27}^+	0.33	0.08	0.36	0.17	-
Na_{35}^+	–0.21	0.02	–0.18	0.04	-
Na_{55}^+	0.18	–0.07	0.17	–0.05	-
	–0.11	–0.07	–0.09	–0.05	0.020
Na_{119}^+	–0.27	–0.14	–0.20	–0.06	-
	0.24	–0.04	0.24	$\sim$	0.004
	–0.04	–0.22	–0.02	–0.18	0.024

3 Calculation scheme

Our approach [20] employs the Kohn-Sham equations for the electronic mean field using the energy-density functional of [18]. The positive ionic background is modeled by a soft jellium density

$$\rho_I(\mathbf{r}) = \frac{\rho_{I0}}{1 + \exp((r - R(\theta))/\alpha)} \tag{6}$$

where quadrupole and hexadecapole axial deformations are introduced through the jellium radius as

$$R(\theta) = R_0 \left[1 + \delta_2 Y_{20}(\theta) + \delta_4 Y_{40}(\theta)\right]. \tag{7}$$

The optimal deformation parameters δ_2 and δ_4 are determined by minimizing the total energy. The continuum is taken into account by a discretization procedure.

We consider the clusters Na_{11}^+, Na_{15}^+, Na_{19}^+, Na_{27}^+, Na_{35}^+, Na_{55}^+, and Na_{119}^+, which, according to jellium estimates [20,22–26], exhibit axial deformations. These clusters represent a broad range of sizes and, as shown in Table 1, cover prolate (Na_{11}^+, Na_{15}^+, Na_{27}^+, Na_{55}^+) and oblate (Na_{19}^+, Na_{35}^+, Na_{119}^+) ground state shapes. Moreover, a few of them (Na_{55}^+ and Na_{119}^+) have shape isomers with a tiny energy deficit $\Delta E \sim 0.02$ eV [20,22] and with quadrupole deformation of opposite sign with respect to the ground state. The largest sample Na_{119}^+ has also a hexadecapole isomer.

Table 1 shows the multipole moments

$$\beta_\lambda = \frac{4\pi}{3} \frac{\int \mathrm{d}\mathbf{r} \rho_0(\mathbf{r}) r^\lambda Y_{\lambda 0}}{N_e \bar{R}^\lambda} \tag{8}$$

with

$$\bar{R} = \sqrt{\frac{5}{3}\overline{r^2}} = \sqrt{\frac{5}{3}\frac{\int \mathrm{d}\mathbf{r}\rho_0(\mathbf{r})r^2}{\int \mathrm{d}\mathbf{r}\rho_0(\mathbf{r})}},$$

where $\lambda = 2, 4$ and $\rho_0(\mathbf{r})$ is the ground state density of valence electrons. The dimensionless multipole moments β_λ are less model dependent because they are computed from expectation values. Thus they can serve for robust characterization of the deformation and for comparison between different models. The quantities δ_λ in the jellium model (6) coincide with the β_λ for small deformation.

The optical response is calculated in the framework of the random phase approximation (RPA). Full RPA for deformed systems is extremely involved. Thus we employ a self-consistent approximation of RPA where the residual interaction is expanded into a sum of separable terms [20]. The expansion employs local one-body operators $Q_{\lambda 1p}(\mathbf{r})$ whose structure is self-consistently designed to map the response mean-field in RPA. The generating operators to which response is explored are chosen to cover the leading multipole operators. The expansion coefficients are computed self-consistently as well. This procedure was shown to provide a sufficiently precise reproduction of the exact residual interaction [20].

For the description of the SM, we used the basis of generating operators

$$\begin{aligned} f_{21p} &= r^{2+p}(Y_{21}(\theta) + Y_{21}^\dagger(\theta)), \qquad p = 0, 2, 4, \\ f_{41p} &= r^{4+p}(Y_{41}(\theta) + Y_{41}^\dagger(\theta)), \qquad p = 0, 2. \end{aligned} \tag{9}$$

The same set of operators was exploited for the description of $\lambda\mu = 21$ branch of the quadrupole plasmon [20]. The close similarity between scissors and quadrupole fields was discussed in [4]. The $p = 0$ component of the input field f_{210} has the form of an external quadrupole field. It generates the leading term of the separable interaction which is peaked at the surface of the system. The next two quadrupole fields ($p = 2$ and 4) lead to separable operators $Q_{21p}(\mathbf{r})$ which are peaked more inside the cluster. We include also hexadecapole fields f_{41p} in order to account for coupling between quadrupole and hexadecapole modes. Such coupling emerges with the onset of deformation, especially in systems having both quadrupole and hexadecapole deformations. The set of the fields (9) delivers good convergence of the separable expansion with respect to the exact results. Explicit expressions for $Q_{\lambda 1p}(\mathbf{r})$ are given in [20].

We study the SM response in terms of photo-absorption. In axially deformed systems, the photo-absorption cross-section from the ground state to an excited state $j = \Lambda^\pi$ of the excitation energy ω_j is

$$\sigma(X\lambda\mu, 0 \to j) = \frac{8\pi^3\lambda+1}{\lambda[(2\lambda+1)!!]^2}\left(\frac{\omega_j}{\hbar c}\right)^{2\lambda-1} |\langle j|\hat{O}^X_{\lambda\mu}|0\rangle|^2 \tag{10}$$

where $\langle j|\hat{O}^X_{\lambda\mu}|0\rangle$ is the reduced transition matrix element and $\hat{O}^X_{\lambda\mu}$ is the operator of electric ($X = E$) or magnetic ($X = M$) transitions. For the SM, we have $\hat{O}^M_{11} = \mu_b \hat{L}_x$. The selections rules are $\mu = \Lambda$ and $(-1)^\lambda = \pi$ for $X = E$ or $(-1)^{\lambda+1} = \pi$ for $X = M$. The electric photo-absorption strength (10) will be used in Section 7 to estimate the competition between the scissors and low-energy electric excitations.

Useful measures for the SM are provided by the sum rules

$$S_m(M1) = \sum_j \omega_j^m B(M1)_j \tag{11}$$

for $m = -1, 0$, and 1. The ratios $\omega = \sqrt{S_1/S_{-1}}$ or $\omega = S_1/S_0$ provide rough estimates for the energy centroid of the low-energy mode. The S_{-1} is proportional to the paramagnetic susceptibility and S_1 to the integral M1 photo-absorption cross-section. The detailed values for the S_m are obtained from explicit RPA results. A simple estimate for S_1 can be obtained using equations (2, 3):

$$S_1(M1) = \sum_j \omega_j B(M1)_j \approx \frac{20.7}{r_s^2} N_e \delta_2^2 \mu_b^2. \tag{12}$$

Sum rules do exist also for electric excitations. The S_1 can be reduced to the simple expression [19]

$$\begin{aligned} S_1(E\lambda) &= \sum_j \omega_j |\langle j|er^\lambda Y_{\lambda\mu}|0\rangle|^2 \\ &= \frac{\hbar^2 e^2}{8\pi m_e}\lambda(2\lambda+1)^2 N_e \overline{r^{2\lambda-2}}. \end{aligned} \tag{13}$$

4 Scissors response

The M1 optical response in light clusters is shown in Figure 2. The present Kohn-Sham calculations yield results close to the ones obtained by using a deformed Woods Saxon potential [4]. Only the excitation energies in prolate clusters are ∼0.2 eV higher, because of the larger quadrupole deformations obtained in the self-consistent approach. The main characteristic of the M1 response is the occurrence of one or two prominent peaks below 1 eV. They are only slightly shifted from their unperturbed $1ph$ (particle-hole) spectrum. In the low-energy region, the $1ph$ $|\Lambda^\pi = 1^+\rangle$ spectrum is very dilute and, therefore, does not meet the conditions for Landau fragmentation or for pronounced coherent superpositions. Because of these features, the low-energy scissors strength can be associated to well defined $1ph$ transitions. In the Nilsson-Clemenger notation $[\mathcal{N}n_z\Lambda]$, they are $[110] \to [101]$ in Na_{11}^+, $[211] \to [202]$ and $[211] \to [200]$ in Na_{15}^+, $[211] \to [220]$ in Na_{19}^+, $[321] \to [310]$ and $[321] \to [312]$ in Na_{27}^+, $[310] \to [321]$ and $[312] \to [321]$ in Na_{35}^+.

As is shown in Figure 2 (compare full and dashed lines), the residual interaction induces a rather moderate blue-shift that is much smaller than *e.g.* the shift for the electric dipole plasmon. The underlying physics is explained in Figure 3 where the exchange-correlations and Coulomb contributions to the leading part of the separable operator $Q_{211}(\mathbf{r})$ are presented for the case of Na_{19}^+ (the repulsive Coulomb is negative in this representation). It is seen that both contributions compensate each other

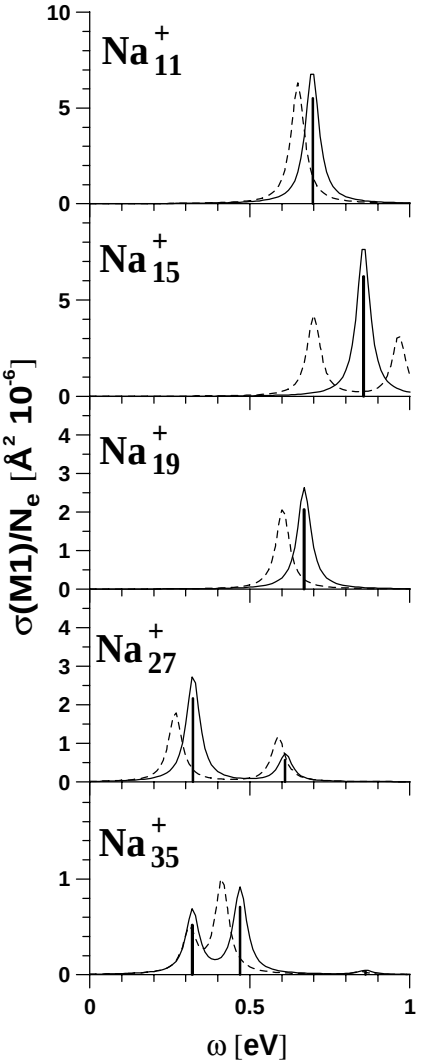

Fig. 2. Photo-absorption cross-section for the scissors mode, weighted by the Lorentz function with the averaging parameter 0.25 eV. The responses with (solid curve) and without (dashed curve) the residual interaction are presented.

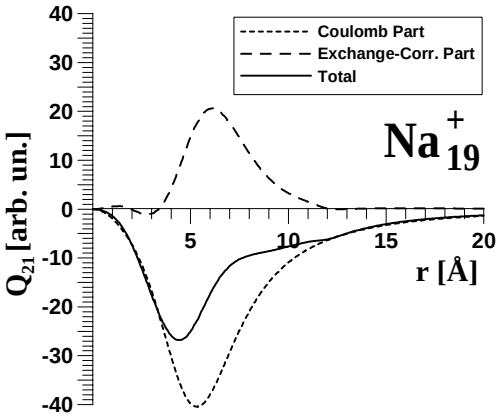

Fig. 3. Radial profile of the residual interaction in Na^+_{19}. Exchange-correlation (long-dashed curve) and Coulomb (shot-dashed curve) contributions are given together with their sum (solid curve).

Table 2. Sum rules S_m (in $eV^m\mu_b^2$) calculated in the energy region 0−6 eV. The fractions for the region 0−1 eV are given in parenthesis.

Cluster	S_{-1}	S_0	S_1
Na^+_{11}	16.5 (92%)	14.7 (72%)	21.5 (34%)
Na^+_{15}	18.7 (84%)	19.2 (69%)	25.9 (43%)
Na^+_{19}	11.3 (98%)	8.2 (90%)	7.4 (67%)
Na^+_{27}	80.6 (96%)	35.6 (74%)	37.7 (25%)
Na^+_{35}	38.9 (97%)	17.2 (84%)	13.3 (43%)
Na^+_{55}	94.9 (97%)	32.6 (78%)	30.2 (26%)
Na^+_{119}	544 (97%)	138 (80%)	103 (36%)

to a large extent. The final outcome is a slight repulsive interaction responsible for the blue-shift. It is worth noting that the balance between these two contributions is rather fragile and can be affected by different factors, *e.g.* triaxiality and detailed ionic structure, making even the sign of the net interaction uncertain [5].

Table 2 collects the calculated scissors strengths summed in the wide (0−6 eV) and low-energy (0−1 eV) regions. It is seen that the $\Delta\mathcal{N} = 0$ low-energy scissors mode, being mainly concentrated below 1 eV, contributes strongly to S_{-1} and S_0. This justifies using S_{-1} and S_0 for a rough estimation of the SM energy as $\omega = \sqrt{S_1/S_{-1}}$ or $\omega = S_1/S_0$. Besides, since S_{-1} is proportional to the paramagnetic susceptibility, this means that just the low-energy SM determines the van Vleck paramagnetism (see discussion in Sect. 6). The high-energy part of the scissors strength (associated with $\Delta\mathcal{N} = 2$ transitions) contributes appreciably to the S_1 sum rule, *i.e.* to the integral M1 photo-absorption cross-section. Table 2 also shows that the increase of the S_m with cluster size is not monotonous. The fluctuations are caused by the predominantly $1ph$ character of the low-energy SM and by the difference in cluster deformations. Na^+_{27} demonstrates especially strong M1 strength, while in oblate clusters Na^+_{19} and Na^+_{35} the strength is relatively weak.

Figure 4 illustrates the coupling of the high-energy scissors branch to the quadrupole plasmon in Na^+_{55}. The correlation between M1 and E2 peaks at ∼3 eV is clearly seen. The coupling of electric and magnetic modes with the same quantum numbers Λ^π is a general feature of deformed finite quantum systems. It is well-known, for example, in atomic nuclei (see, *e.g.* [9,27]).

The coupling of the SM with dipole and spin-dipole oscillations in clusters was discussed in detail in reference [5]. In particular, it was shown that breaking the symmetry by the ionic lattice results in a weak coupling between these oscillations of the opposite space parity. This feature may change for clusters deposited on a surface since symmetry breaking there is even stronger.

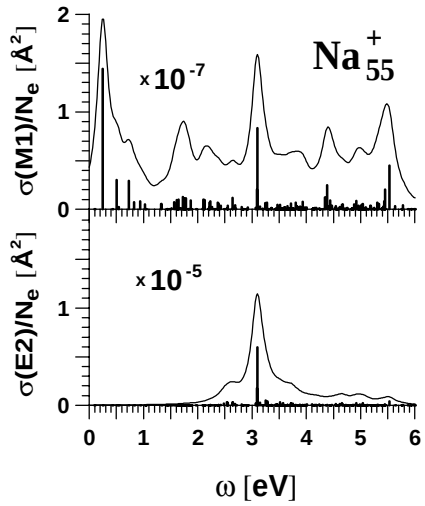

Fig. 4. Coupling between the high-energy scissors branch and E2 quadrupole plasmon in prolate Na_{55}^{+}. M1 and E2 photoabsorptions are weighted by the Lorentz function with the averaging parameter 0.25 eV.

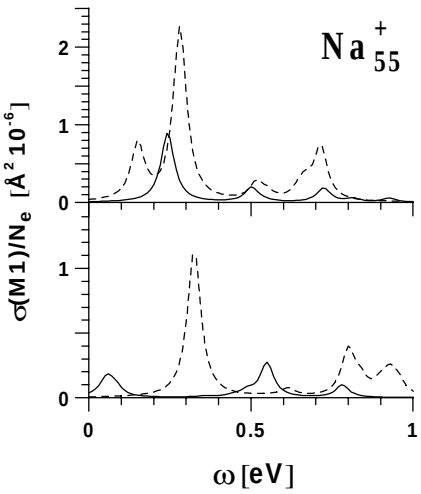

Fig. 5. The strength distribution of the scissors modes in Na_{55}^{+}, built on the prolate ground state (upper panel) and oblate first isomer (lower panel). Jellium (solid curve) and ionic (dashed curve) SRPA results are compared.

5 Effects of shape isomers and ionic structure

The calculations [20,22] show that light axially deformed clusters ($N_e < 40$) have one distinct minimum corresponding to the ground-state deformation. The heavier clusters ($40 < N_e < 100$) have usually two minima with opposite quadrupole deformations (prolate and oblate) and very close energies. The energy difference between the ground and the shape isomeric states is often less than 0.02 eV = 200 K. The number of shape isomers with a tiny energy deficit increases with cluster size. These isomers may have a variety of very different shapes. Significant amounts of isomers can be found in a thermal ensemble and thus contribute to the SM, *e.g.*, at room temperature.

Figure 5 compares the scissors modes built on the ground and isomeric states in Na_{55}^{+}. Both of them show rich spectra of low-lying M1 states. But the character of the spectra and strength distribution differs substantially. To explain the differences, one should take in to account that the M1 spectra are generated by several $1ph$ M1 transitions between the levels in the vicinity of the Fermi surface. Prolate and oblate shapes yield different sequences of the single-particle levels near the Fermi surface. As a result, some of the $1ph$ M1 transitions significant in the prolate case are transformed to $1pp$ or $1hh$ transitions in the oblate case, thus strongly decreasing the strength.

Figure 5 compares also the SRPA results obtained with the soft jellium model (6) as well as with detailed ionic structure [5]. In the case of the ionic structure, the global cluster deformations slightly deviate from those in the jellium case. It is seen that calculations with the ionic structure give somewhat different positions of the SM peaks with respect to the jellium case. Such a redistribution of the peaks is due to different energies of the single-particle levels in the ionic calculations. The photo-absorption response in the ionic case is stronger, which is also explained by the redistribution of the levels in the mean field. The level sequence in this case favors a few more $1ph$ transitions of M1 type.

Altogether, the calculations demonstrate some important points concerning the SM in clusters of a medium size:

(i) the mode is distributed over several $1ph$ transitions;
(ii) the single-particle spectrum near the Fermi level is rather dense and so even small changes in the calculation scheme can redistribute visibly the spectrum and open (or close) some relevant $1ph$ transitions;
(iii) as was mentioned above, the ground and first isomeric states in medium-size clusters can be very close in energy. So, the SM in free medium-size clusters should be considered as a statistical mixture of contributions from different shapes (predominantly of the ground state and first isomer). A similar argument (involving the deformation splitting, Landau fragmentation and contributions of shape isomers) was recently used to explain the experimental E1 optical response in deformed sodium clusters with $50 < N_e < 60$ [22].

Less shape isomerism will be provided by the SM in metal clusters deposited on insulating substrates [28]. These clusters are oblate and their mean size and magnitude of the deformation can be well controlled. Such clusters seem to be the most promising systems for experimental search of the SM.

6 Magnetic anisotropy

The static orbital magnetism in clusters was widely studied during the last decades. The studies were mainly based on the Landau theory of the atomic magnetism [29]. Applied to clusters, they covered a variety of issues: giant dia- and para-magnetism in weak magnetic fields [30,31], size and temperature effects [32,33], manifestation of quantum supershells in magnetic susceptibility [33], influence

of cluster shape (both axial and triaxial) on the magnetic properties [1,2], anisotropy of magnetic susceptibility in deformed clusters [1,2], orbital magnetism of supported clusters [3], etc. The relation of the van Vleck paramagnetism with the SM was established in [1].

Despite all these studies, some subtle and interesting points of the orbital magnetism were not yet considered. In this section we will discuss the new effect of dia-para anisotropy in the magnetic susceptibility, which can be found in particular light sodium clusters. RPA calculations [4] show that the SM energies and B(M1) strengths scale with the deformation δ_2 and the electron number $N_{\rm e}$, basically according to the trends (2) and (3). Strong fluctuations, however, take place in small clusters [4]. They reflect the $1ph$ nature of the transitions and may affect the magnetic susceptibility thus causing in particular cases the dia-para anisotropy.

The interaction of cluster valence electrons with a uniform magnetic field B_k applied along the coordinate axis k is

$$\hat{H}_{\rm int} = \mu_b B_k \hat{L}_k + \frac{1}{2}\mu_b^2 B_k^2 \rho_k^2 \tag{14}$$

where $k = x, y, z$ is the coordinate index, $\hat{L}_k = \sum_{a=1}^{N_{\rm e}} \hat{L}_k^{(a)}$ is the kth projection of the angular moment operator (the sum runs over all valence electrons), $\rho_z^2 = \sum_{a=1}^{N_{\rm e}}(x_a^2 + y_a^2)$, $\rho_x^2 = \sum_{a=1}^{N_{\rm e}}(y_a^2 + z_a^2)$, and $\rho_y^2 = \sum_{a=1}^{N_{\rm e}}(x_a^2 + z_a^2)$. We neglected in (14) electron spins because their contribution to the magnetic susceptibility is expected to be sufficiently small for the clusters considered below (axial sodium clusters with even $N_{\rm e}$ and completely filled Fermi level).

If the magnetic field is weak, one can use the perturbation theory. Up to the second order to B_k, the induced change of the ground state energy is

$$\omega_0^{\rm int} = \mu_b B_k \langle 0|\hat{L}_k|0\rangle - \mu_b^2 B_k^2 \sum_{j\neq 0} \frac{|\langle j|\hat{L}_k|0\rangle|^2}{\omega_j} + \frac{1}{2}\mu_b^2 B_k^2 N_e \overline{\rho_k^2} \tag{15}$$

where ω_j is the energy of the excited state $|j\rangle$ and $\overline{\rho_k^2}$ is the average value of ρ_k^2. The negative second and positive third terms in (15) are responsible for the temperature independent van Vleck paramagnetism and Langevin diamagnetism, respectively.

The first linear term in (15) dominates in systems with a partly filled Fermi level because in this case we have not the complete mutual compensation of the contributions of valence electrons with different orbital projections Λ. The linear term then leads to strong paramagnetic moments $\mu = \mu_b|\Lambda|$ in axial clusters with odd $N_{\rm e}$ [2]. In magic spherical clusters where the Fermi level is fully occupied, both the first linear and second quadratic terms are zero and the clusters are thus diamagnetic [2]. Such diamagnetism is called giant [31] since, due to $\overline{\rho_k^2} \gg a_0^2$ (a_0 is the Bohr radius), it is much stronger than the atomic one.

We will consider z-axial deformed clusters with even N_e and fully occupied Fermi level. In this case, the linear term in (15) is zero and the van Vleck contribution takes place for $k = x, y$ only. The orbital magnetic susceptibility $\chi_k = -\partial^2\omega_0^{\rm int}/\partial B_k^2$ is then the sum of the Langevin diamagnetic and van Vleck paramagnetic terms:

$$\chi_k = \chi_k^{\rm dia} + \chi_k^{\rm para}, \tag{16}$$

where

$$\chi_k^{\rm dia} = -\mu_b^2 N_e \overline{\rho_k^2\rangle} = -\mu_b^2 \Theta_k^R, \tag{17}$$

$$\chi_k^{\rm para} = 2\mu_b^2 \sum_{j\neq 0} \frac{|\langle j|\hat{L}_k|0\rangle|^2}{\omega_j} = \mu_b^2 \Theta_k, \tag{18}$$

having denoted by

$$\Theta_k = 2\sum_{j\neq 0} \frac{|\langle j|\hat{L}_k|0\rangle|^2}{\omega_j} \tag{19}$$

and

$$\Theta_k^R = N_e \overline{\rho_k^2} \tag{20}$$

the cranking and rigid moments of inertia, respectively.

Note that for $k = x, y$ the operator entering into the matrix element in (18) is exactly the scissors generator. This hints that just the low-energy SM mainly contributes to $\chi_{x,y}^{\rm para}$. Indeed, Table 2 shows that the contribution of the low-energy scissors mode to the value $S_{-1} \sim \chi_k^{\rm para}$ achieves 85−100%. So, the SM dominates the van Vleck paramagnetism.

In the schematic model [1], the moment of inertia acquires the rigid-body value such that $\Theta_{x,y} = \Theta_{x,y}^R$ and thus $\chi_{x,y}^{\rm para} = -\chi_{x,y}^{\rm dia}$, *i.e.* we have a complete compensation of dia- and paramagnetic terms in (16). Due to the axial symmetry, one also has $\chi_z^{\rm para} = 0$. The total susceptibility becomes, therefore, strictly anisotropic [1]

$$\chi_x = \chi_y = 0, \qquad \chi_z = \chi_z^{\rm dia}, \tag{21}$$

varying from zero to diamagnetic values.

On the other hand, strong shell effects in particular light clusters may alter appreciably the above result. This is illustrated for Na_{27}^+ in Figure 6. The SM in this cluster has very low excitation energy (see Fig. 2) and an exceptionally large value of S_{-1} (see Tab. 2). Thus the paramagnetic susceptibility is enhanced considerably and is no longer compensated by the diamagnetic term. So, Na_{27}^+ should be paramagnetic in x, y-directions and diamagnetic in z-direction. The cluster Na_{11}^+ also hints this property.

The competition between dia- and paramagnetic contributions to the magnetic susceptibilities χ_k was quantitatively considered earlier in the Kohn-Sham-Nilsson model [2]. Nearly a complete balance $\chi_{x,y}^{\rm para} = -\chi_{x,y}^{\rm dia}$ was found for the axial cluster Na_{26} while other even axial clusters were shown to exhibit a steady diamagnetism. This result evidently correlates with our calculations. Besides, the dia-para anisotropy in Na_{27}^+ was earlier predicted in the Woods-Saxon model [14]. The fact that quite different models yield similar results for Na clusters with $N_e = 26$

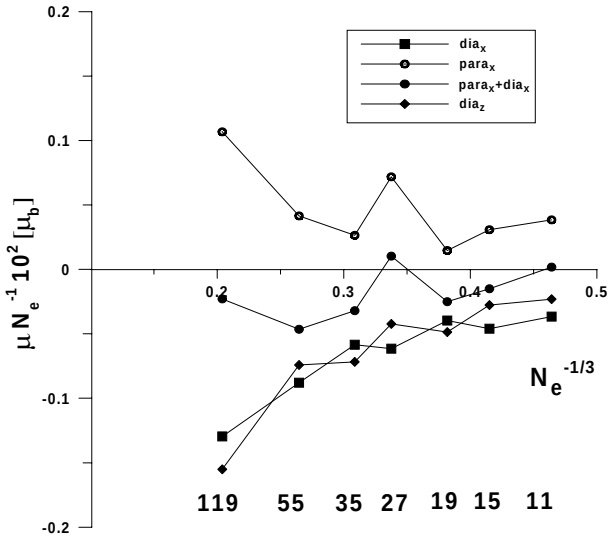

Fig. 6. Normalized diamagnetic, paramagnetic and summed moments $\mu = \chi B_k$ ($B_k = 4$ T) in axial deformed clusters Na_{11}^+, Na_{15}^+, Na_{19}^+, Na_{27}^+, Na_{35}^+, Na_{55}^+ and Na_{119}^+.

means that the dia-para anisotropy in Na_{27}^+ can be indeed the case. The magnetic moments in Na_{27}^+ are sufficiently large to be measured. Observation of the dia-para anisotropy would provide a strong (though indirect) evidence of the SM in clusters.

7 Experimental perspectives

7.1 General analysis

As was mentioned in the introduction, the SM is not yet observed experimentally in metal clusters. The search of the SM is hindered by several factors:

(1) the mode has very low photo-absorption cross-section. Following our results, in Na clusters with $N_e \simeq 10{-}10^2$, $\sigma(M1)/N_e \simeq 10^{-5}{-}10^{-7}$ Å^2 as compared to $\sigma(E1)/N_e \simeq 2$ Å^2 for the dipole plasmon. Such a weak M1 signal is at the edge of the sensitivity of modern detectors;

(2) equations (10–13) allow to estimate the ratios for the maximal optical responses as

$$\sigma(E1)/\sigma(M1) = 0.35 \times 10^5 \text{ Å}^{-2} \left(\frac{r_s}{\delta_2}\right)^2 \qquad (22)$$

and (for $\omega_{E2} \simeq 3$ eV [19,20])

$$\sigma(E2)/\sigma(M1) = 0.82 \times 10^{-2} \text{ Å}^{-4} \left(\frac{r_s^2}{\delta_2}\right)^2 N_e^{2/3}. \quad (23)$$

This gives for deformed ($\delta_2 = 0.2$) sodium ($r_s = 2.1$ Å) clusters $\sigma(E1)/\sigma(M1) \simeq 4 \times 10^6$ and $\sigma(E2)/\sigma(M1) \simeq 10^2$ (the latter for $N_e = 125$). So, the SM suffers from the competition with E1 and E2 strengths. Besides, the competition with E2 increases with cluster size. The above estimates compare the SM optical response with the maximal responses of E1 and E2 plasmons. As is shown in the next subsection, the competition is much weaker in the low-energy region where the SM has its stronghold, but one has still to be aware of large amounts of E1 strength;

(3) the low-energy SM lies in the infrared region where commonly used detectors are not efficient enough;

(4) the SM energy decreases with cluster size and reaches the region of phonon excitations, ∼0.1 eV in clusters with $N_e \sim 10^3$ [34];

(5) at the first glance, temperature effects may hinder the SM. Indeed, the typical temperature is ∼100 K $\simeq$ 0.01 eV. In deformed clusters with $N_e = 10^3{-}10^4$, such a temperature is larger than the average energy-level spacing ($\sim 10^{-4}$ eV). So the temperature-independent van Vleck paramagnetism provided by the SM should transfer to the temperature-dependent Curie one. However, this does not mean the disappearance of the SM but only the reduction of the SM contribution to χ_k^{para}. What is more important, the temperature is safely below the SM energy and so the SM mode should survive. Indeed, the SM is determined by the deformation splitting (which can be fixed and kept large, see below the discussion for deposited clusters) but not by the energy-level spacing.

In spite of the hindrances listed above, clusters offer enough opportunities to look for the optimal conditions for observing the SM: one may change cluster size and (or) deformation, use different metals, choose between free and supported clusters, etc. The macroscopic estimates (2–3) and the present jellium RPA calculations may serve as a guide. The corresponding analysis is done below. Sodium clusters with a moderate deformation $\delta_2 = 0.2$ are considered as a typical example. Following the estimation (2), their SM energy is $\omega \simeq 1 \times N_e^{-1/3}$ eV.

Heavy clusters look promising because the M1 photo-absorption cross-section grows linearly with size. Already in deformed clusters with $N_e = 10^4{-}10^6$ the scissors signal should be detectable. Unfortunately, the corresponding energy $\omega \simeq 0.05{-}0.01$ eV approaches and even enters the region of phonon excitations. Thus the best compromise for free sodium clusters is achieved at the size of several thousands atoms. Besides that, these clusters are large enough to ensure the dominance of the orbital scissors mode over spin M1 excitations.

We may also look for clusters of larger density and deformation to increase the energy and the strength of the mode. For example, Li clusters ($r_s = 1.7$ Å) allow one to increase both the energy and optical response by a factor of ∼1.5 with respect to Na ($r_s = 2.1$ Å). Further improvement may be achieved with Ag ($r_s = 1.6$ Å), Mg ($r_s = 1.4$ Å), or Al ($r_s = 1.1$ Å). In any case, highly deformed clusters are welcome because $\sigma(M1) \sim \delta_2^2$ and $\omega \sim \delta_2$.

In general, free clusters seem not suitable for observing the SM. They are well mass-separated only up to sizes of hundred atoms. However, these systems have a weak M1 signal. As for heavier clusters, they suffer from

a poor mass separation and are expected to be weakly deformed [26]. Moreover, as was discussed in Section 5, their M1 signal is a statistical mix of contributions of different shapes given by the ground state and isomers.

Deposited clusters look more promising. One can adopt techniques that allow to get oblate clusters (Na and Ag) on dielectric surfaces [28] and, more remarkably, to monitor their size and deformation. Clusters with 10^2-10^6 atoms can be used for this aim. In this way, one can obtain supported clusters of a desired size and shape. High density of clusters on the surface gives good statistics in the measurements. Last but not least, monitoring the shape of clusters gives the chance to use the trends $\sigma(M1) \sim \delta_2^2$ and $\omega_{M1} \sim \delta_2$ to distinguish the SM from the E1 and E2 signals. To this end, one has to irradiate clusters of the same size but of different deformations. Then the low-energy E1 and E2 cross-sections are also affected but, hopefully, in an irregular fashion. Thus their signal should be averaged out or at least show trends which differ from that of the SM. The cross-sections measured at different deformations can be mutually subtracted to extract a small, and yet useful, signal. For the analysis of such experiments, we need accurate theoretical estimates accounting for all the main factors and, in particular, for the influence of the surface on the electric and scissors plasmons. Such work is in progress.

The competition with E1 and E2 modes may be suppressed partially by resorting to specific reactions and techniques capable of hindering if not suppressing the E1 and E2 channels. We will discuss this issue for three relevant reactions: photo-absorption, resonance Raman scattering, and inelastic electron scattering.

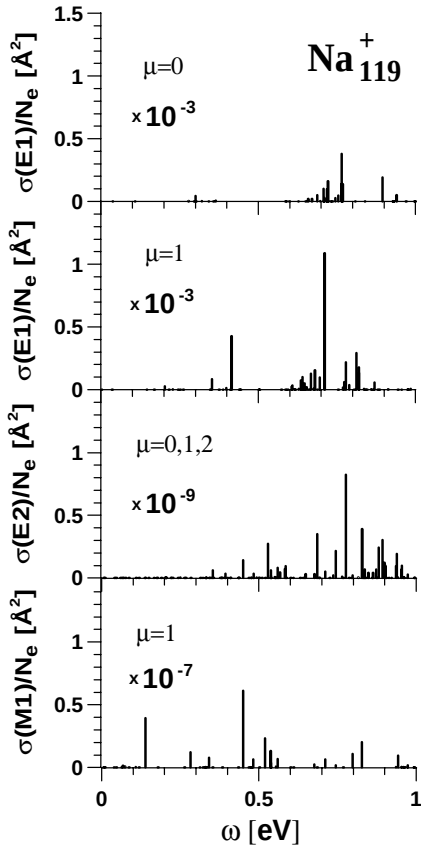

Fig. 7. Photo-absorption E1, E2 and scissors cross-sections in Na^+_{119} weighted by the Lorentz function with the averaging parameter 0.25 eV. The E1 $\mu = 0$ and 1 branches are given separately to show their relative contributions to the competition with the scissors mode.

7.2 Photo-absorption

The SM lies much lower than the dipole and quadrupole plasmon modes (0.2−1.0 eV against 2.5−3.0 eV for the dipole and 2−4 eV for the quadrupole plasmons [19,20]). In principle, one could exploit this energy separation to focus on the SM. However, its M1 photo-absorption cross-section is still very small as compared to the E1 strength and it can be masked by the tail of close-by E1 modes. This is illustrated in Figure 7 which compares E1, E2 and M1 photo-absorption strengths calculated within the SRPA approach [20] in the axially deformed ground state of Na^+_{119}. The E1 strength, although extremely small compared to the dipole plasmon peak, is still strong enough to mask the SM. The influence of the quadrupole E2 strength in Na^+_{119} is negligible (but may be stronger in heavier clusters).

The competition with the E1 channel can be decreased by using deformed (oblate) clusters with $N \simeq 10^3-10^4$ atoms, supported on dielectric surfaces, and adopting infrared techniques with the polarized light. For the SM, the magnetic field of the incoming light should be parallel to the surface. This can be done with both *s*- and *p*-polarizations (with the electrical field perpendicular and parallel to the incident plane, respectively). The *s*-polarized light under an angle $\sim 0°$ with the surface normal suppresses the $\mu = 0$ E1 branch without weakening the SM. The *p*-polarized light at angle $\sim 90°$ suppresses the $\mu = 1$ E1 branch, again without weakening the SM. The second variant seems to be preferable since the $\mu = 1$ branch is generally stronger (see, *e.g.*, Fig. 7). Unfortunately, the polarization does not allow suppression of both dipole branches simultaneously. It only weakens but does not avoid completely the strong competition with the dipole excitations.

7.3 Resonant Raman scattering

In resonance Raman scattering (inelastic scattering of polarized photons), the SM may be populated through the de-excitation of the dipole plasmon excited by the incoming photon. The difference between energies of incoming and outgoing photons gives the energy of the SM. One needs to look at E1 decays, which represent the leading channel and may populate in deformed systems M1 and E2 states. With respect to photo-absorption, resonance Raman scattering has the advantage of excluding the competition with the strong E1 mode and to work with visible light. An experiment of this kind was carried

out on supported Ag clusters [35]. The analysis of the data suggested, however, that the E2 rather than the SM was populated through the E1 decay. On the other hand, it is not simple to separate E2 and M1 modes which are mixed in deformed systems.

7.4 Inelastic electron scattering

Inelastic electron scattering is also a promising technique. At backward scattering angles, the M1 signal can prevail over the electric ones. This property enabled the discovery of the scissors mode in deformed atomic nuclei [8]. Polarization of the electrons provides additional possibilities to extract the magnetic response. In nuclear physics, electrons with very high energies (tens and hundreds MeV) are used, which favors creation of well collimated, intense and monochromatic electron beams. Moreover, at such high energies, there is no problem enhancing sufficiently the relative contribution of the transversal form factor.

The low-energy electron beams and the angular resolved techniques, suitable for our purpose, are now available in the framework of the electron energy loss spectroscopy (EELS), see, *e.g.* [36]. To our knowledge, EELS was not used so far for observation in metal clusters of any plasmons except the dipole one. At the same time, theoretical estimates [37–39] show that at certain scattering angles the dipole contribution can be well suppressed in favor of the quadrupole plasmon, which, therefore, can be observed. From the latter analysis, we may infer that also the SM may be extracted. Indeed, in the low-energy region the SM can be stronger excited in the photo-absorption than the E2 mode.

8 Conclusions

The scissors mode (SM) in axially deformed sodium clusters has been studied within a self-consistent RPA approach based on the soft jellium model for the ionic background and density-functional theory for the electrons. The calculations show that the distribution of the low-energy scissors strength is dominated by $1ph$ states with only small shifts by the residual interaction. The SM thus reflects almost directly the density of $1ph$ M1 transitions near the Fermi surface and exhibits an extreme sensitivity to the actual deformation. The SM is rather unambiguous in light clusters ($N_e < 40$) while it should be a statistical mix of contributions from different shapes in heavier clusters. Furthermore, the high-energy branch of the SM in deformed systems is coupled with the quadrupole plasmon.

The calculations show that the SM determines the van Vleck paramagnetism and results in a strong anisotropy of the magnetic susceptibility. Moreover, due to quantum shell effects, some clusters (Na_{27}^{+}) demonstrate dia-para anisotropy where the axial cluster is diamagnetic along the symmetry axis and paramagnetic along the other two axes. The magnetic moments are large enough to be measured. The experimental observation of the dia-para anisotropy, being interesting itself, could also serve as an indirect evidence of the SM in clusters.

A general analysis of possible routes for experimental observation of the scissors mode was presented. Photo-absorption with polarized light, inelastic electron scattering and Raman scattering were considered. The electron scattering seems to be the most promising tool. Moreover, deposited clusters favor the detection of the SM as compared to free ones. Its features need yet to be worked out in detail. Work in that direction is in progress.

The work was partly supported (V.O.N.) by RFBR (00-02-17194), Heisenberg-Landau (Germany-BLTP JINR) and DFG (436RUS17/102/01) grants.

References

1. E. Lipparini, S. Stringari, Phys. Rev. Lett. **63**, 570 (1989); Z. Phys. D **18**, 193 (1991)
2. S. Frauendorf, V.V. Pashkevich, S.M. Reimann, Surf. Rev. Lett. **3**, 441 (1996)
3. C. Binns, Surf. Sci. Rep. **44**, 1 (2001)
4. V.O. Nesterenko, W. Kleinig, F.F. de Souza Cruz, N. Lo Iudice, Phys. Rev. Lett. **83**, 57 (1999)
5. P.-G. Reinhard, V.O. Nesterenko, E. Suraud, S. El Gammal, W. Kleinig, Phys. Rev. A **66**, 013206 (2002)
6. V.O. Nesterenko, J.R. Marinelli, F.F. de Souza Cruz, W. Kleinig, P.-G. Reinhard, Phys. Rev. Lett. **85**, 3141 (2000)
7. N. Lo Iudice, F. Palumbo, Phys. Rev. Lett. **41**, 1532 (1978)
8. D. Bohle *et al.*, Phys. Lett. B **137**, 27 (1984)
9. N. Lo Iudice, Phys. Part. Nucl. Phys. **28**, 556 (1997)
10. Ll. Serra, A. Puente, E. Lipparini, Phys. Rev. B **60**, R13966 (1999)
11. A. Minguzzi, M.P. Tosi, Phys. Rev. A **63**, 023609 (2001)
12. D. Guéri, S. Stringari, Phys. Rev. Lett. **83**, 4452 (1999)
13. O.M. Maragó, S.A. Hopkins, J. Artl, E. Hodby, G. Hechenblaikner, C.J. Foot, Phys. Rev. Lett. **84**, 2056 (2000)
14. V.O. Nesterenko, W. Kleinig, F.F. de Souza Cruz, J.R. Marinelli, in *Proceedings of Intern. Symposium on Cluster and Nanostructure Interfaces*, Richmond, USA, 1999, edited by P. Jena, S.N. Khanna, B.K. Rao (World Scientific, Singapure, 2000), p. 209
15. V.O. Nesterenko, W. Kleinig, F.F. de Souza Cruz, N. Lo Iudice, in *Proceedings of Intern. Workshop "Collective excitations in Fermi and Bose Systems"*, Serra Negra, San Paulo, Brazil, 1998, edited by C.A. Bertulani, L.F. Canto, M.S. Hussein (World Scientific, Singapore, 1999), p. 225
16. V.O. Nesterenko, W. Kleinig, in *Proceedings of Intern. Symposium "Similarities and Differences between Atomic Nuclei and Clusters"*, Tsukuba, Japan, 1997, edited by Y. Abe, I. Arai, S.M. Lee, K. Yabana, AIP Confer. Proceed. **416**, 77 (1998)
17. P.-G. Reinhard, O. Genzken, M. Brack, Ann. Phys. (Lpg) **5**, 576 (1996)
18. O. Gunnarsson, B.I. Lundqvist, Phys. Rev. B **13**, 4274 (1976)

19. V.O. Nesterenko, W. Kleinig, V.V. Gudkov, N. Lo Iudice, Phys. Rev. A **56**, 607 (1997)
20. W. Kleinig, V.O. Nesterenko, P.-G. Reinhard, Ann. Phys. (N.Y.) **297**, 1 (2002)
21. W. Kleinig, V.O. Nesterenko, P.G. Reinhard, Ll. Serra, Eur. Phys. J. D **4**, 343 (1998)
22. V.O. Nesterenko, W. Kleinig, P.G. Reinhard, Eur. Phys. J. D **19**, 57 (2002)
23. S.M. Reinmann, S. Frauendorf, M. Brack, Z. Phys. D **34**, 125 (1995)
24. C. Yannouleas, U. Landman, Phys. Rev. B **51**, 1902 (1995)
25. Th. Hirschmann, B. Montag, J. Meyer, Z. Phys. D **37**, 63 (1996)
26. S. Frauendorf, V.V. Pashkevich, Ann. Phys. (Lpg) **5**, 34 (1996)
27. J. Kvasil, N. Lo Iudice, V.O. Nesterenko, M. Kopal, Phys. Rev. C **58**, 209 (1998)
28. T. Wenzel, J. Bosbach, A. Goldman, F. Stietz, F. Träger, Appl. Phys. B **69**, 513 (1999); J. Bosbach, D. Martin, F. Stietz, T. Wenzel, F. Träger, Appl. Phys. Lett. **69**, 2605 (1999)
29. L.D. Landau, Z. Phys. **64**, 629 (1930)
30. A.I. Buzdin, O.V. Dolgov, Yu. E. Lozovik, Phys. Lett. A **100**, 261 (1984)
31. V. Kresin, Phys. Rev. B **38**, 3741 (1988)
32. J.M. van Ruitenbeek, D.A. van Leewen, Phys. Rev. Lett. **67**, 640 (1991)
33. S. Frauendorf, V.M. Kolomietz, A.G. Magner, A.I. Sanzhur, Phys. Rev. B **58**, 5622 (1998)
34. P.-G. Reinhard, E. Suraud, Eur. Phys. J. D **21**, 315 (2002)
35. H. Portales, E. Duval, L. Saviot, M. Fujii, M. Sumitomo, S. Hayashi, Phys. Rev. B **63**, 233402 (2001)
36. Y. Chen, J.C. Barnard, R.E. Palmer, M.O. Watanabe, T. Sasaki, Phys. Rev. Lett. **83**, 2406 (1999); B.J. Eves, F. Festy, K. Svensson, R.E. Palmer, Appl. Phys. Lett. **77**, 4223 (2000); R.E. Palmer, B.J. Eves, F. Festy, K. Svensson, Surf. Sci. **502-503**, 224 (2002)
37. T.L. Ferrell, P.M. Echenique, Phys. Rev. Lett. **55**, 1526 (1985)
38. W. Ekardt, Phys. Rev. B **32**, 1961 (1985); *ibid.* B **33**, 8803 (1986); *ibid.* B **36**, 4483 (1987)
39. L.G. Gerchikov, A.N. Ipatov, A.V. Solov'ev, W. Greiner, J. Phys. B **31**, 3065 (1998)